BIOCHEMISTRY
including biophysical chemistry & molecular biology

Article

pubs.acs.org/biochemistry

Visible Light Induction of an Electron Paramagnetic Resonance Split Signal in Photosystem II in the S_2 State Reveals the Importance of Charges in the Oxygen-Evolving Center during Catalysis: A Unifying Model

Johannes Sjöholm, Stenbjörn Styring, Kajsa G. V. Havelius,[†] and Felix M. Ho*

Photochemistry and Molecular Science, Department of Chemistry, Ångström Laboratory, Uppsala University, P.O. Box 523, SE-751 20 Uppsala, Sweden

ABSTRACT: Cryogenic illumination of Photosystem II (PSII) can lead to the trapping of the metastable radical $Y_Z^{\bullet}$, the radical form of the redox-active tyrosine residue D1-Tyr161 (known as Y_Z). Magnetic interaction between this radical and the $CaMn_4$ cluster of PSII gives rise to so-called split electron paramagnetic resonance (EPR) signals with characteristics that are dependent on the S state. We report here the observation and characterization of a split EPR signal that can be directly induced from PSII centers in the S_2 state through visible light illumination at 10 K. We further show that the induction of this split signal takes place via a Mn-centered mechanism, in the same way as when using near-infrared light illumination [Koulougliotis, D., et al. (2003) *Biochemistry 42*, 3045−3053]. On the basis of interpretations of these results, and in combination with literature data for other split signals induced under a variety of conditions (temperature and light quality), we propose a unified model for the mechanisms of split signal induction across the four S states (S_0, S_1, S_2, and S_3). At the heart of this model is the stability or instability of the $Y_Z^{\bullet}(D1\text{-}His190)^+$ pair that would be formed during cryogenic oxidation of Y_Z. Furthermore, the model is closely related to the sequence of transfers of protons and electrons from the $CaMn_4$ cluster during the S cycle and further demonstrates the utility of the split signals in probing the immediate environment of the oxygen-evolving center in PSII.

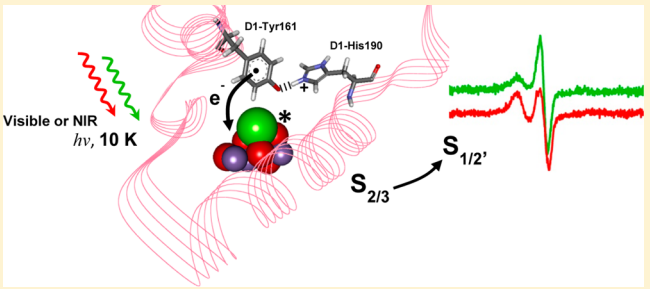

In oxygenic photosynthesis in higher plants, algae, and cyanobacteria, the water splitting reaction is catalyzed by the enzyme Photosystem II (PSII), a multisubunit transmembrane protein located in the thylakoid membranes of the organism.[1] The catalytic center at which this takes place is known as the oxygen-evolving complex (OEC), which consists of a $CaMn_4$ metal cluster and a nearby D1-Tyr161, commonly termed Y_Z. When light is absorbed by the chlorophyll assembly P_{680} in PSII, charge separation takes place. After excitation, P_{680}* transfers an electron to the acceptor side of PSII via cofactors $Pheo_{D1}$, Q_A, and Q_B, and further to the rest of the electron transport chain. The electron hole that is left on P_{680}^+ as a result of this electron transfer is filled by donation of an electron from Y_Z.[2] Concomitant with oxidation of Y_Z, the phenolic proton moves in a hydrogen bond toward D1-His190,[3,4] creating the neutral radical $Y_Z^{\bullet}$ and a charged $(D1\text{-}His190)^+$ residue.[5,6] $Y_Z^{\bullet}$ is in turn re-reduced by donation of an electron from the $CaMn_4$ cluster. After four light-induced charge separation events, four oxidation equivalents accumulate on the $CaMn_4$ cluster. This leads to the oxidation of substrate water that is bound to the $CaMn_4$ cluster to give molecular O_2, and a return of the cluster to its most reduced state.[7]

According to the Kok model[8] (and the recent extended versions thereof[9,10]), the stepwise oxidation of the $CaMn_4$ cluster during the water oxidation process is represented by the S cycle, which consists of a number of metastable intermediate states of the cluster, known as S_n states (n = 0−4). While the S_0 state is the least oxidized form of the cluster, it is the S_1 state that prodominates after dark adaptation of PSII. After absorption of one or two photons, charge separation originating at P_{680} advances the $CaMn_4$ cluster to the metastable S_2 or S_3 state, respectively. Oxidation of the S_3 state leads to the formation of the unstable S_4 state that spontaneously oxidizes water to O_2, and a return to the S_0 state, without further light-induced charge separation.[7]

The $Y_Z^{\bullet}$ radical can be observed as a metalloradical CW-EPR signal by interaction with the $CaMn_4$ cluster. This type of signal, also termed a split EPR signal, was first observed in PSII samples incapable of oxygen evolution (depleted of calcium or chloride or treated with fluoride, acetate, or ammonia) by illumination above 250 K.[11−17] In recent years, split EPR signals have been reported also for oxygen-evolving PSII. These signals are induced by illumination under cryogenic (<20 K) conditions,[18−24] and their spectral properties are dependent upon the S state of the $CaMn_4$ cluster at the time of

Received: October 14, 2011
Revised: February 13, 2012
Published: February 21, 2012

illumination. The $Y_Z^{\bullet}$ radical is formed via light-induced charge separation at high quantum yields[24] and inasmuch as 40−50% of the PSII centers,[22,24,25] even at such low temperatures.[26] While the reduction of $Y_Z^{\bullet}$ by the $CaMn_4$ cluster occurs extremely rapidly under physiological conditions (nanosecond to millisecond time scale[27−29]), it is proposed that this process is blocked under cryogenic conditions, so that the lifetime of $Y_Z^{\bullet}$ becomes sufficiently long for the interaction signals to be observed.

Of the split signals reported for intact PSII samples, the split S_1, split S_3, and split S_0 signals can be induced by visible light illumination at 5−20 K.[20,22−24,30] It has also been shown that a split signal can be induced from S_2 state centers by visible light illumination, but only if the sample had first been illuminated at higher temperatures (77−190 K).[31] In addition, near-infrared (NIR) light has been reported to induce split signals from the S_2 and S_3 states.[18,21,30,32] As P_{680} does not absorb NIR radiation, it has been proposed that NIR induction of the split signal arises from direct excitation of one or more Mn ions in the $CaMn_4$ cluster rather than through P_{680}-centered charge separation. The excited cluster oxidizes Y_Z to $Y_Z^{\bullet}$ even at cryogenic temperatures, and as a result, the cluster itself goes back one step in the S cycle (i.e., $S_2{}^*Y_Z \rightarrow S_1Y_Z^{\bullet}$ and $S_3{}^*Y_Z \rightarrow S_2'Y_Z^{\bullet}$, with S_2' denoting a S_2 center that is deficient in one proton because of the pure electron transfer nature of this "back-reaction"). Only very recently was it shown that the induction mechanism for the split S_3 signal is the same independent of the wavelength of the incident light.[25]

In this paper, we report for the first time the direct induction of a split signal by visible light illumination of an S_2 state sample at 10 K and distinguish this signal from the visible light-induced split S_1 signal. We also compare these split signals with that induced by NIR illumination of S_2 state centers. These signals are termed the $(S_2)^{VIS}$, $(S_1)^{VIS}$, and $(S_2)^{NIR}$ split signals, where the S state in which the PSII sample was initially poised is indicated in parentheses and the light used for split signal illumination denoted by superscript text. Combining these results with literature data for the induction and characteristics of the other known split signals, we propose a unified model for the induction mechanism of these signals that correlates closely with the alternating pattern of release of electrons and protons from the $CaMn_4$ cluster during the S cycle. It is proposed that the key to understanding the mechanism through which a particular split signal can be induced lies in the stability of the $Y_Z^{\bullet}(D1\text{-}His190)^+$ pair in the presence of the S state in question.

MATERIALS AND METHODS

Preparation of PSII Membranes. PSII-enriched membranes were prepared from spinach under dim green light according to the method described in ref 33, with modifications described in ref 34. Concentrated stock samples of PSII membranes (~6−8 mg of Chl/mL) were suspended in buffer [25 mM MES-NaOH (pH 6.3), 400 mM sucrose, 5 mM $MgCl_2$, and 10 mM NaCl] and stored at −80 °C before being used. Oxygen evolution rates of 400 ± 20 μmol of O_2 (mg of Chl)$^{-1}$ h^{-1} were obtained in the presence of 0.5 mM PpBQ under saturating light conditions. The Chl concentration was determined according to the method described in ref 35.

Synchronization of the $CaMn_4$ Cluster to the S_1 and S_2 States. PSII membranes were diluted to 1.9−2.0 mg/mL with buffer (above) and filled in calibrated EPR tubes. Samples were illuminated with room light at 20 °C for 2 min to fully oxidize Y_D before being dark-adapted for 15 min at room temperature. A single preflash (Nd:YAG laser, 532 nm, 6 ns, Spectra Physics, Newport) was then applied to each sample before further dark adaptation at room temperature, in the absence of an electron acceptor. This protocol synchronizes all the $CaMn_4$ clusters to the dark-stable S_1 state.[36]

The protocol of ref 37 was used for optimized synchronization of PSII centers to the S_1 and S_2 states for cryogenic EPR measurements. Briefly, the exogenous electron acceptor PpBQ was added in the dark to preflashed samples to a final concentration of 0.5 mM [stock solution in DMSO, final DMSO concentration of 3% (v/v)]. After being mixed for 30 s at room temperature, the sample was transferred to a 1 ± 1 °C ethanol bath and allowed to equilibrate in the dark for a further 1.5 min. To obtain the S_2 state, the samples were immediately given one turnover laser flash after equilibration in the ethanol bath and then frozen within 1−2 s in a 200 K dry ice/ethanol bath. Samples were then stored in liquid nitrogen until EPR measurements were taken. Where the S_1 state was required, no turnover laser flash was given, and the 1 °C ethanol bath-equilibrated samples were frozen directly in the dry ice/ethanol bath before being transferred to liquid nitrogen. Where indicated, an illumination at 200 K of the samples prior to EPR measurements was done in a dry ice/ethanol bath with saturating light for 4 min. After illumination, the samples were quickly transferred to liquid nitrogen (77 K).

For the study of S state-dependent oscillation of the S_2 multiline signal, the higher S states were obtained in the same manner as described above, with the exception that two, three, four, five, and six turnover flashes (at 1.25 Hz flash frequency) were applied to the 1 °C equilibrated samples. Samples dominated by the S_3, S_0, S_1, S_2, and S_3 states, respectively, were thus obtained.

EPR Measurements and Split Signal Induction. EPR measurements were performed with a Bruker ELEXYS E500 spectrometer, equipped with a SuperX EPR049 microwave bridge and a Bruker SHQ4122 cavity. The system was fitted with a liquid helium cryostat and temperature controller (ITC503) from Oxford Instruments Ltd. Spectrometer settings are given in the figure legends.

The split signals were induced at 10 K by illumination of the S state-synchronized PSII membranes directly in the EPR cavity. For visible illumination, the light was provided by a 150 W projector lamp fitted with a neutral density filter (10% T, Schott NG9). The light was filtered through a 5 cm thick $CuSO_4$ solution and directed into the cavity using a transparent perspex light guide. The intensity measured at the position of the cavity window was 20 W/m^2. For NIR illumination, 830 nm light was provided by a continuous laser diode (LQC830-135E, Newport) and directed into the cavity after passing through a beam spreader. The light intensity at the cavity window was 67 W/m^2.

RESULTS AND DISCUSSION

Direct Induction of Split Signals from the S_2 State at 10 K. PSII samples synchronized to the S_2 state were illuminated with either visible light or NIR light at 10 K to induce the $(S_2)^{VIS}$ or $(S_2)^{NIR}$ split signal, respectively (note that no preillumination was applied before split signal induction, cf. ref 31). The results are shown in Figure 1A, where the $(S_1)^{VIS}$ split signal induced and measured under the same spectrometer conditions is also presented for comparison. To exclude contributions from stable radicals (e.g., chlorophyll and carotenoids) induced by the cryogenic illumination but

dx.doi.org/10.1021/bi2015794 | Biochemistry 2012, 51, 2054−2064

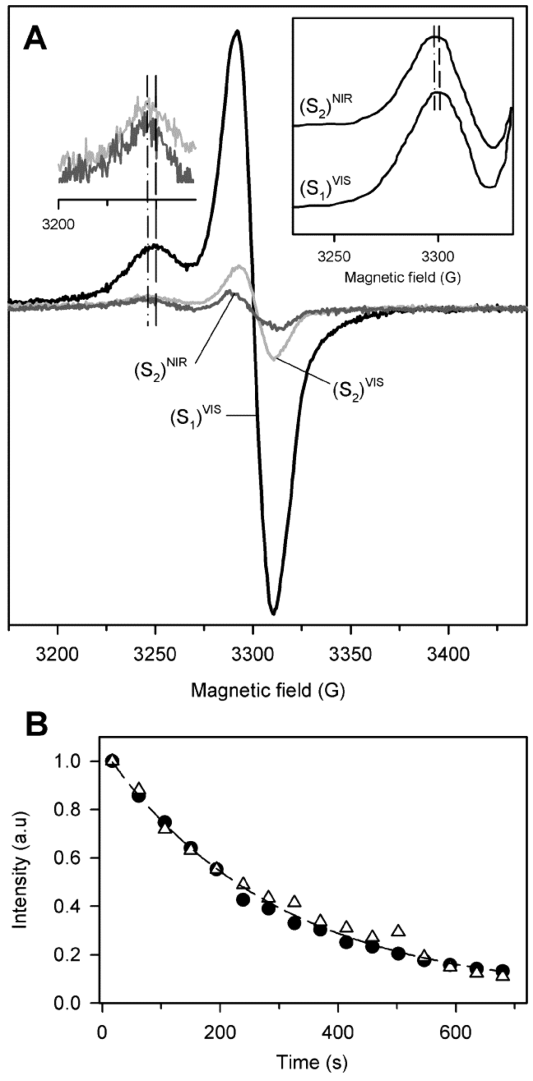

Figure 1. Split signals induced by illumination at 10 K of PSII membranes poised in the S_1 and S_2 states. (A) EPR spectra from the decaying part of the visible light-induced split signal from the S_1 [$(S_1)^{VIS}$, black] and S_2 [$(S_2)^{VIS}$, light gray] states (shown as light-minus-postdecay spectra) and the NIR-induced split signal from the S_2 state [$(S_2)^{NIR}$, dark gray] (shown as a light-minus-dark spectrum). For comparison, the $(S_2)^{VIS}$ and $(S_2)^{NIR}$ signals are also shown with the intensity expanded by a factor of 5. The field positions of the respective low-field peaks are indicated with a dashed [$(S_1)^{VIS}$] or dashed–dotted [$(S_2)^{VIS}$ and $(S_2)^{NIR}$] line. The inset shows the low-field peak of the split signals induced by NIR light in an S_2 sample and visible light in an S_1 sample replotted from ref 18. Adapted with permission from ref 18. Copyright 2003 American Chemical Society. (B) Normalized amplitude changes of the decaying part of the $(S_1)^{VIS}$ (●) and $(S_2)^{VIS}$ (△) split signals measured in the dark after induction (measured at the low-field peak indicated in panel A). The dashed line is a single-exponential decay fit with a $t_{1/2}$ of 3.3 min. EPR conditions: microwave frequency of 9.27 GHz, microwave power of 16 mW, field modulation frequency of 100 kHz, modulation amplitude of 10 G, and temperature of 10 K.

otherwise unrelated to the split signal,[23,25] light-minus-postdecay spectra were calculated, where "postdecay" signifies the spectrum obtained after dark adaptation (>15 min) of the illuminated sample at 10 K. This subtraction isolates the metastable split signal ($t_{1/2} \sim 3.5$ min[23,24]) in the resulting difference spectrum, removing the contribution from the dark-stable radicals. The decay kinetics of the $(S_1)^{VIS}$ and $(S_2)^{VIS}$ signals are shown in Figure 1B. As can be seen, these split signals have very similar decay half-times ($t_{1/2} \sim 3.3$ min), and are consistent with previous literature results. By contrast, an ordinary light-minus-dark spectrum could be used for investigations of the $(S_2)^{NIR}$ split signal, as the side radicals are not induced by NIR light, and the resulting split signal is also stable in the dark.[25,30,32]

Comparing the $(S_2)^{VIS}$, $(S_2)^{NIR}$, and $(S_1)^{VIS}$ split signals, we can see that their spectral shapes are very similar. In each case, a radical-like derivative signal is observed at ~3300 G, accompanied by a smaller positive peak further downfield, at ~3250 G. The $(S_2)^{VIS}$ and $(S_2)^{NIR}$ signals have much lower intensities than the $(S_1)^{VIS}$ signal.

The $(S_2)^{VIS}$ Signal Is Not Due to Residual S_1 State Centers. The induction of a split signal from the S_2 state by NIR illumination [i.e., the $(S_2)^{NIR}$ signal] has previously been reported and is generally thought to result in the $S_1Y_Z^{\bullet}$ redox state.[18] However, given the extremely similar line shapes of all three signals shown here, it is tempting to conclude that the $(S_2)^{VIS}$ signal reported here merely results from residual S_1 state centers in the sample. However, we have previously shown that it is possible to achieve a miss-free $S_1 \rightarrow S_2$ transition by careful control of the conditions of the flash turnover protocol.[37] This protocol was used for sample preparation here. In the forthcoming discussion, we will argue that while the $(S_2)^{VIS}$ signal originates from $S_1Y_Z^{\bullet}$, it is induced from S_2 state centers via a Mn-centered mechanism.

A number of other experimental results demonstrate that residual S_1 centers are not the source of the observed split $(S_2)^{VIS}$ signal. First, evidence that the $(S_2)^{VIS}$ signal is associated with illumination of S_2 state centers is found in the comparison of the spectral shapes of the three split signals (Figure 1A). Closer inspection of the smaller peak at 3250 G reveals that while the $(S_2)^{VIS}$ and $(S_2)^{NIR}$ signals share the same peak position, it is shifted approximately 3–4 G downfield compared with that of the $(S_1)^{VIS}$ split signal. This shift is reproducible across multiple samples. Indeed, a careful examination of the data presented in ref 18, where the $(S_2)^{NIR}$ signal was first reported, shows that such a downfield shift compared to the $(S_1)^{VIS}$ signal was also present there (inset of Figure 1A). This suggests that while the interactions between the species responsible for the split signal (i.e., $Y_Z^{\bullet}$ and the $CaMn_4$ cluster) are very similar, there is a small but consistent spectral difference when the split signal is induced from the S_2 rather than the S_1 state.

Furthermore, determination of the microwave power at half-saturation ($P_{1/2}$) of the $(S_1)^{VIS}$, $(S_2)^{VIS}$, and $(S_2)^{NIR}$ split signals showed a clear distinction between the split signals induced from the S_2 state and that induced from the S_1 state. The data are shown in Figure 2 and summarized in Table 1. The intensity of the split signal at each microwave power was measured as the height of the respective downfield positive peaks at 3250 G, and the value of $P_{1/2}$ was obtained by a least-squares fit of the data according to eq 1:

$$I = \frac{K\sqrt{P}}{\sqrt{\left(1 + \frac{P}{P_{1/2}}\right)^{b}}} \quad (1)$$

where I is the measured intensity at applied microwave power P, b is the inhomogeneity constant, and K is a constant of

dx.doi.org/10.1021/bi2015794 | Biochemistry 2012, 51, 2054–2064

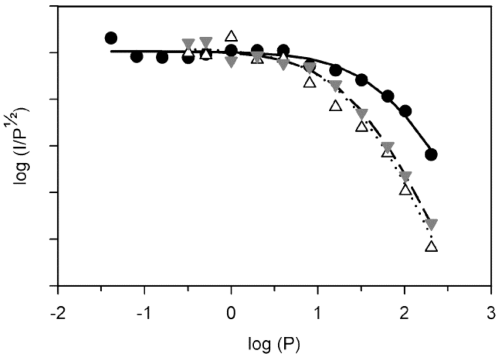

Figure 2. Microwave power dependence of the $(S_1)^{VIS}$ (●), $(S_2)^{VIS}$ (△), and $(S_2)^{NIR}$ (▼) split signals. The respective difference spectra were calculated as described in the legend of Figure 1, at varying microwave powers. The intensity at each microwave power was measured at the downfield peaks (indicated in Figure 1A). The curves were obtained by a least-squares fit of the data according to eq 1. EPR conditions were as described in the legend of Figure 1, except with a microwave power of 0.04−200 mW.

Table 1. Microwave Powers at Half-Saturation ($P_{1/2}$) of the $(S_1)^{VIS}$, $(S_2)^{VIS}$, and $(S_2)^{NIR}$ Split EPR Signals

signal	$P_{1/2}$ (mW)[a]
$(S_1)^{VIS}$	74 ± 9^b
$(S_2)^{VIS}$	$35 \pm 8^{b,c}$
$(S_2)^{NIR}$	36 ± 7^c

[a]The range of $P_{1/2}$ values obtained from separate samples is given as the uncertainty. [b]$P_{1/2}$ determined from the decaying part of the light-induced signal. [c]The $P_{1/2}$ values include both untreated samples and samples given an extra 200 K illumination.

proportionality.[38,39] A b value of 1 was used, as is commonly found in the literature (i.e., assuming total inhomogeneity of the spin's magnetic environment[40]). In addition, to exclude the possibility of S_1 state contamination despite our use of the miss-free $S_1 \rightarrow S_2$ flash transition protocol, additional S_2 samples that had been prepared by laser flash turnover were illuminated with white light at 200 K to convert any possible remaining S_1 state centers to the S_2 state.[36,37,41,42] Measurements for establishing the $P_{1/2}$ value (for both visible and NIR illumination for split signal induction) were then repeated using these samples. It can be seen from Table 1 that while the $P_{1/2}$ values are the same for both the $(S_2)^{VIS}$ and $(S_2)^{NIR}$ split signals, including the samples illuminated at 200 K, the $P_{1/2}$ value of the $(S_1)^{VIS}$ split signal is approximately twice as large.

Additional evidence of the direct involvement of S_2 centers in induction of the $(S_2)^{VIS}$ signal is a decrease in the S_2 multiline signal intensity observed upon induction of the $(S_2)^{VIS}$ signal. The S_2 state exhibits a distinctive multiline signal ($S = {}^1/_2$) that has often been used for quantification of the S state distribution in a sample.[36,41] Panels A and B of Figure 3 show the S_2 multiline signal intensity of two series of samples given zero to six laser flashes. For both series, deep period-of-four oscillation patterns were found, indicative of the very good quality of the samples and the flash protocol used. The multiline intensity was measured before and during split signal illumination with either NIR (Figure 3A) or visible (Figure 3B) light. It was found that the S_2 multiline signal intensity was reduced in all samples during cryogenic illumination. Interestingly, the extent of the reduction in intensity was essentially the same irrespective of the light used [Figure 3A,B (△)]. On the basis of the multiline intensities for the samples exposed to one (Figure 3C) or five turnover flashes, the reduction in the intensity of the S_2 multiline signal was found to involve ∼18% of the available S_2 state centers. The reduction can be seen as a reverted multiline signal in the light-minus-dark difference spectra for both visible and NIR light illumination (Figure 3D, black spectra). Furthermore, difference spectra recorded over a wider magnetic field range showed that the observed reductions in multiline signal intensity were not due to any light-induced changes in the $g \sim 4$ region (ref 43 and data not shown). This is consistent with the very low temperature used during illumination.[43,44]

Significantly, when the samples were allowed to adapt to the dark for >30 min after the end of either visible or NIR illumination, the light-minus-dark difference spectra of the S_2 multiline remained unchanged (Figure 3D, gray spectra). This is despite the fact that the $(S_2)^{VIS}$ signal decayed in the dark (Figure 1B). This decay can also be seen in Figure 3D (marked with an asterisk).

Taken together, the $P_{1/2}$ data and the changes in the S_2 multiline signal upon cryogenic illumination directly link the $(S_2)^{VIS}$ split signal to S_2 state centers. In particular, the lack of recovery of the intensity of the multiline signal during the decay of the S_2 split signal in the $(S_2)^{VIS}$ sample suggests a persistent loss of S_2 state centers after cryogenic illumination. This is mechanistically very significant and is discussed in more detail below.

The Mn-Centered Mechanism Operates for Both $(S_2)^{VIS}$ and $(S_2)^{NIR}$ Split Signals. The persistent reduction in the S_2 multiline signal intensity is a strong argument for the Mn-centered mechanism for the induction of both the $(S_2)^{VIS}$ and $(S_2)^{NIR}$ split signals reported here. This is because such a reaction, i.e., $S_2{}^*Y_Z \rightarrow S_1Y_Z^{\bullet}$, would lead to the appearance of a split signal, followed by a permanent reduction in the number of S_2 centers in the sample after a subsequent $S_1Y_Z^{\bullet}$ $(R^-) \rightarrow S_1Y_Z$ (R) recombination (R signifies a recombination partner, such as Q_A^- [25,32]). Had the split signal been induced via the P_{680}-centered mechanism, $S_2Y_Z^{\bullet}$ would have formed, and the decay of the split signal would have occurred via the $S_2Y_Z^{\bullet}$ $(R^-) \rightarrow S_2Y_Z$ (R) recombination instead, allowing the intensity of the S_2 multiline signal to recover. This was not the observed behavior.

Whereas for the $(S_2)^{NIR}$ split signal no recombination partner is available, thus explaining its stability,[18,26,45] formation of Q_A^- from P_{680}-centered charge separation can take place when visible light is used. This is possible in parallel to the Mn excitation giving rise to the $(S_2)^{VIS}$ signal, and Q_A^- is the most likely candidate for being recombination partner R in the reaction scheme described above.[24] This has also been demonstrated for the split S_3 signals,[25,32] where both NIR and visible light illumination of S_3 centers gave split signal induction via the Mn-centered mechanism. Signal decay was, however, only observed where visible illumination generated Q_A^- in parallel, or where Q_A^- was preformed before NIR illumination.[25,32] Such behavior is in contrast to that of the S_0 and S_1 states, where NIR illumination does not lead to any formation of split signals.[24,25]

Therefore, we propose here that the same Mn-centered mechanism operates for split signal induction with visible and NIR light illumination of PSII in the S_2 state at 10 K. Independent of wavelength used, the species formed is $S_1Y_Z^{\bullet}$. Further support for this is found in the essentially identical peak positions and $P_{1/2}$ values for both the $(S_2)^{VIS}$ and $(S_2)^{NIR}$ split

dx.doi.org/10.1021/bi2015794 | Biochemistry 2012, 51, 2054−2064

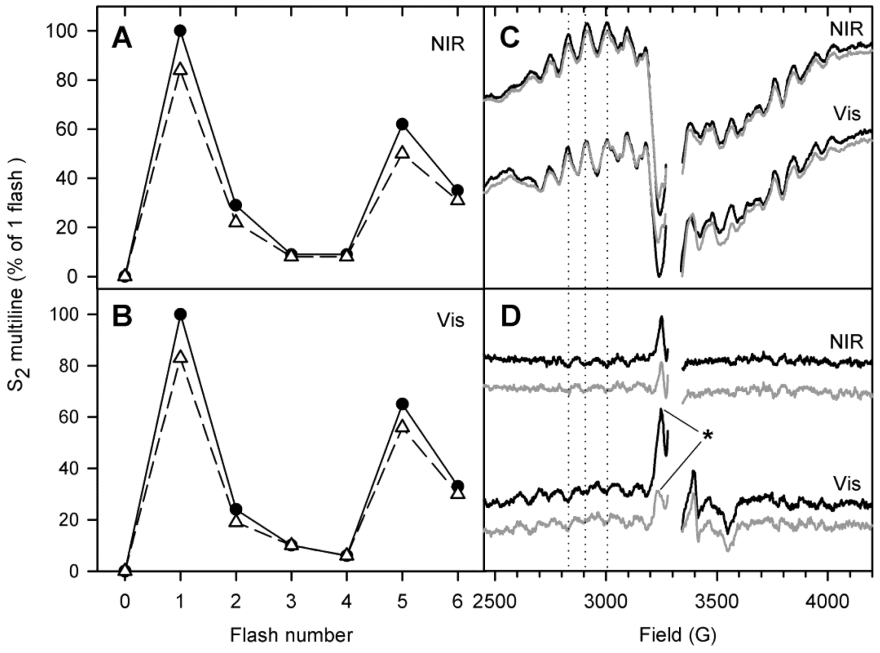

Figure 3. S_2 multiline signals in samples subjected to visible or NIR illumination at 10 K. (A) Oscillation of the S_2 multiline signal after zero to six flashes measured in the dark (●) or during NIR light illumination (△). (B) Oscillation of the S_2 multiline signal after zero to six flashes measured in the dark (●) or during visible light illumination (△). (C) S_2 multiline signals of samples given one turnover flash measured before (black) or during (gray) either NIR or visible light illumination. (D) Light-minus-dark difference spectra of the S_2 multiline signal (black) and the change in the multiline signal after dark adaptation for >30 min (i.e., postdecay-minus-dark, gray). The asterisk indicates the loss of $(S_2)^{VIS}$ split signal amplitude during dark adaptation. The dotted lines indicate the field positions used for quantification of the S_2 multiline signal presented in panels A and B. EPR conditions: microwave frequency of 9.27 GHz, microwave power of 16 mW, field modulation frequency of 100 kHz, modulation amplitude of 14 G, and temperature of 10 K.

Table 2. Comparison of the Split Signal Induction with Direct Illumination at 10 K across the S States

	S_0		S_1		S_2		S_3	
	split signal?	species formed	split signal?	species formed	split signal?	species formed	split signal?	species formed
visible light illumination	yes	$S_0Y_Z^\bullet$	yes	$S_1Y_Z^\bullet$	yes	$S_1Y_Z^\bullet$	yes	$S_2Y_Z^\bullet$
NIR light illumination	no	–	no	–	yes	$S_1Y_Z^\bullet$	yes	$S_2Y_Z^\bullet$
mechanism	P_{680}-centered		P_{680}-centered		Mn-centered		Mn-centered	

Scheme 1. S State Cycle of the $CaMn_4$ Cluster[a]

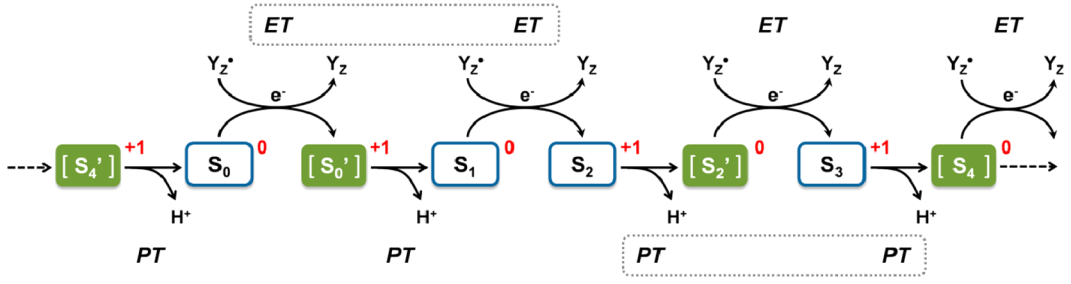

[a]The scheme shows the different S states (filled boxes) and the presumed intermediates between them (empty boxes). Electron (ET) and proton (PT) transfers during the transitions between the different S states are indicated. State S_1 is set to a relative charge of 0, and the charges of the remaining intermediates are indicated in relation to this. Electron transfer is the subsequent step after the S_0 and S_1 states (dashed box ET). In contrast, proton transfer follows the S_2 and S_3 states (dashed box PT).

signals (Figure 1 and Table 1). The similar line shapes of these split signals compared with the $(S_1)^{VIS}$ split signal are reasonable, given that the resulting interaction is between $Y_Z^\bullet$ and the S_1 state in all cases. The variations in $P_{1/2}$ values may stem from differences in the protein environment that surrounds the S_1 and S_2 states before cryogenic illumination. Although the $CaMn_4$ structures in the S_1 and S_2 states are essentially identical,[46] the S_2 state is more positively charged by comparison. It is therefore conceivable that the protein environments surrounding the cluster in the S_1 and S_2 states are not identical (e.g., due to electrostriction[47]). This could change the spin−lattice relaxation properties of the system, thereby giving rise to the S state-dependent $P_{1/2}$ values despite $S_1Y_Z^\bullet$ being formed in both cases. Such small differences in the protein environment may also result in slight alterations in the

dx.doi.org/10.1021/bi2015794 | Biochemistry 2012, 51, 2054−2064

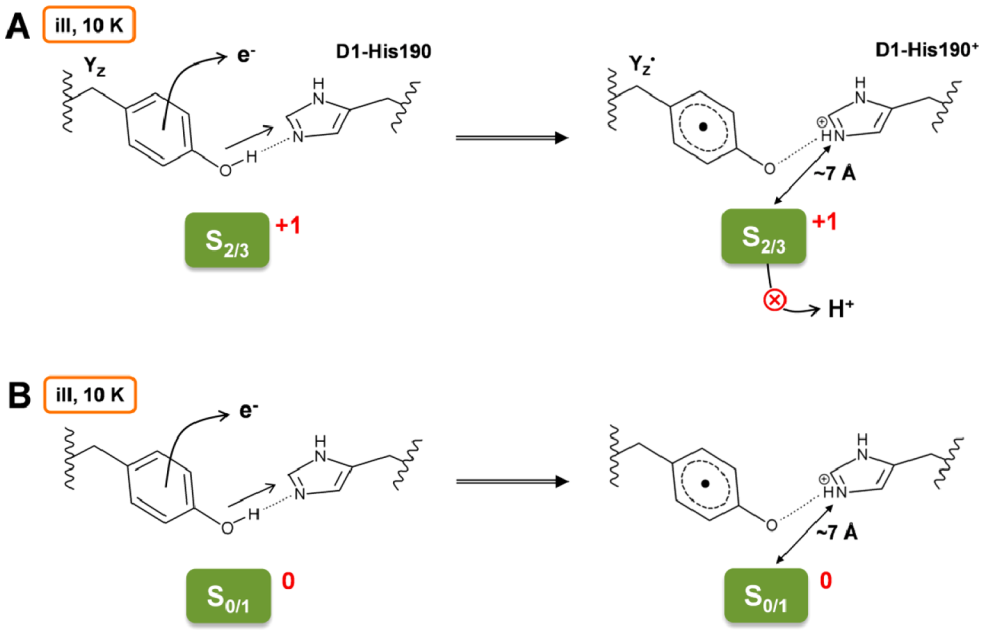

Figure 4. Electrostatic environment of the $Y_Z^{\bullet}$ radical formed upon P_{680}-centered charge separation. The electron and proton movements associated with Y_Z oxidation upon illumination with visible light at 10 K are shown in the reaction schemes. (A) Transfer of electrons and protons from Y_Z leads to the formation of the $Y_Z^{\bullet}(His190)^+$ pair situated ~7 Å from the $CaMn_4$ cluster. The subsequent release of a proton from the $CaMn_4$ cluster is however blocked at the cryogenic temperature used, leading to a conservation of the higher charge (+1) at the cluster after visible light illumination of PSII in the S_2 or S_3 state. This leads to unfavorable repulsion between the $Y_Z^{\bullet}(His190)^+$ pair and the cluster. (B) The relative charge of the $CaMn_4$ cluster in the S_0 or S_1 state is lower (0), leading to less electrostatic repulsion when the $Y_Z^{\bullet}(His190)^+$ pair is formed by illumination at 10 K.

magnetic coupling between $Y_Z^{\bullet}$ and the $CaMn_4$ cluster, explaining the minor shift observed in the peak positions.

Comparison between Split Signal Induction Mechanisms and the S Cycle. Our current report of a $(S_2)^{VIS}$ split signal completes the range of split signals that can be directly induced by <20 K cryogenic visible light illumination of PSII to all four stable S states. The light quality capable of inducing each signal and the mechanism by which $Y_Z^{\bullet}$ formation proceeds are summarized in Table 2. As a result of the addition of our current $(S_2)^{VIS}$ signal with the conclusion that the mechanism by which it is formed is not P_{680}-centered, it can be seen that the split signal induction behavior from the S states can be neatly classified into two groups.

For the S_2 and S_3 states, the $CaMn_4$ cluster is sensitive to both visible and NIR light at cryogenic temperatures, and split signal induction proceeds via a Mn-centered mechanism for both light qualities. By contrast, split signals are only induced by P_{680}-centered charge separation in the more reduced S_0 and S_1 states. Given these observations, are there any common traits within these two groups of S states that can be identified?

An interesting pattern emerges when Table 2 is compared with the pattern of release of electrons and protons from the $CaMn_4$ cluster during the S cycle (Scheme 1). As proposed in ref 10, redox leveling of the $CaMn_4$ cluster is required to allow one and the same tyrosine residue Y_Z to function as the oxidant throughout the S cycle. This is achieved by a strictly alternating release of electrons and protons for charge balance. Together with the well-established data for the proton release pattern (refs 10 and 48 and references therein) and the pH dependence[49,50] of the S state transitions, the transitions can be divided into electron-only ($S_1 \rightarrow S_2$), proton-first ($S_2 \rightarrow S_3$, $S_3 \rightarrow [S_4]$), and electron-first ($S_0 \rightarrow S_1$) transitions (Scheme 1). As such, for the S states where the mechanism for split signal formation at cryogenic temperatures is a P_{680}-centered mechanism (S_0 and S_1), the next step in the S cycle involves an electron transfer. By contrast, where the Mn-centered mechanism prevails (S_2 and S_3), the upcoming step is a proton transfer.

At first sight, the above correlation suggests that transfers of electrons and protons from the $CaMn_4$ cluster govern whether the induction of a split signal occurs via "forward" or "backward" electron transfer. However, note that even though transfers of electrons and protons from Y_Z are possible at 10 K (indeed, that is the basis for the metastability of $S_nY_Z^{\bullet}$ and thus the appearance of split signals), transfers of both electrons and protons from the $CaMn_4$ cluster is considered to be completely blocked below 20 K across all S states. Therefore, whether a release of a electron or proton from the $CaMn_4$ cluster is to occur upon the next S state transition cannot be the decisive factor for the observed pattern. Instead, a model focusing on the electrostatic environment of the $CaMn_4$ cluster is proposed below. Applications of this model to two sets of data in the literature are then presented to illustrate the utility of this model in explaining experimental observations.

A Unified Model for the Split Signal Induction Mechanisms. We propose here a unifying model that is able to rationalize the observed split signal induction behavior across the different S states. This model focuses on the stability of $Y_Z^{\bullet}$ induction through cryogenic illumination, with the key consideration being the surrounding electrostatic environment in each of the S states. The alternating electron and proton release pattern of the S cycle (Scheme 1) remains of central significance, as well as the blockage of transfer of a proton from the $CaMn_4$ cluster under cryogenic conditions.

Upon oxidation of Y_Z by P_{680}^+, the phenolic proton is transferred to D1-His190 across the strong hydrogen bond between these residues,[3,4] resulting in a $Y_Z^{\bullet}(His190)^+$ pair (Figure 4). As the $S_1 \rightarrow S_2$ transition is an electron-only

dx.doi.org/10.1021/bi2015794 | Biochemistry 2012, 51, 2054−2064

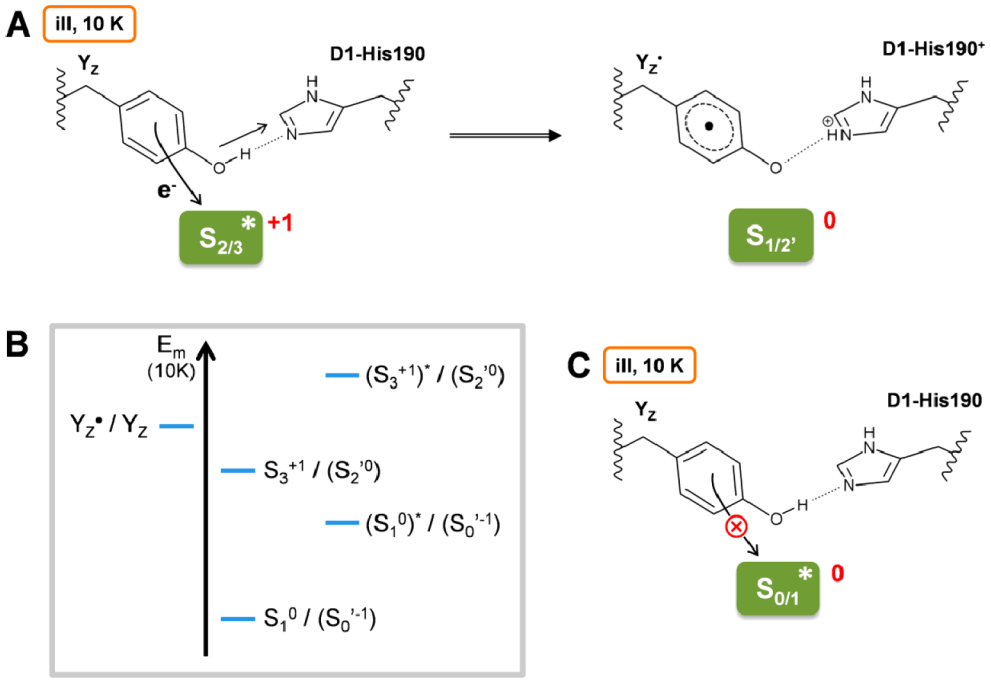

Figure 5. Induction of the split S_2 and S_3 signals via the Mn-centered mechanism as understood on the basis of the stability of $Y_Z^\bullet(His190)^+$ pair formation, as well as the relative redox potential of $Y_Z^\bullet/Y_Z$ and the cluster. (A) Upon cryogenic illumination of the S_2 and S_3 states at 10 K, an electron is transferred from Y_Z to the excited $CaMn_4$ cluster, lowering the charge of the cluster that lies in the proximity of the $Y_Z^\bullet(His190)^+$ pair thus formed. (B) Representation of the relative reduction potentials at 10 K of the ground S state redox couples, $S_3^+/S_2'^0$ and $S_1^0/S_0'^{-1}$, and the excited S state redox couples, $(S_3^+)^*/S_2'^0$ and $(S_1^0)^*/S_2'^{-1}$, in relation to the potential of $Y_Z^\bullet/Y_Z$. The asterisk indicates that the $CaMn_4$ cluster is excited due to cryogenic illumination, and the prime indicates an S state with a protonation state different from that of the corresponding native S states (see Scheme 1). An analogous pattern of changes in reduction potential applies to the S_2^+/S_1^0 and $(S_2^+)^*/S_1^0$ couples as for the $S_3^+/S_2'^0$ and $(S_3^+)^*/S_2'^0$ couples, respectively. (C) In the lower S states (S_0 and S_1), the excited $CaMn_4$ cluster remains insufficiently oxidizing to oxidize $Y_Z^\bullet$.

transition,[10] the charge of the $CaMn_4$ cluster in the S_2 and S_3 states is +1, higher relative to that of the S_1 and S_0 states (Scheme 1 and Figure 4). This means that, for S_2 and S_3 state centers, a $Y_Z^\bullet(His190)^+$ pair that is formed would be situated in the proximity (~7 Å[51]) of a more highly charged $CaMn_4$ cluster compared with the case of S_0 or S_1 centers (Figure 4). Because both theory and experiments[28,52] have suggested that electrostatic interaction acts as the trigger for the release of H^+ from the cluster, this proximity to a more positively charged cluster is consistent with the model for the S cycle in which the S_2 and S_3 transitions are proton-first transitions.[10]

The lack of split signal induction from the S_2 and S_3 states via the P_{680}-centered mechanism can then be understood if the release of a proton from the $CaMn_4$ cluster is blocked at the cryogenic temperatures used (Figure 4A). Preventing this proton release leads to the higher charge of the S_2 and S_3 states being maintained, so that the $Y_Z^\bullet(His190)^+$ pair is not (meta)stably formed, because of unfavorable electrostatic interactions between the two positively charged species.[a] As a result, no P_{680}-centered split signal formation is seen for the S_2 and S_3 states, even though P_{680}^+ is formed from visible light illumination, e.g., during $(S_2)^{VIS}$ induction.

For the S_0 and S_1 states, on the other hand, the charge of the $CaMn_4$ cluster is lower, such that the same degree of electrostatic repulsion between $Y_Z^\bullet(His190)^+$ and the cluster is not present (Figure 4B). This is also in agreement with the observation that the next step in the S cycle for the S_0 and S_1 states is an electron transfer, so the formation of the $Y_Z^\bullet(His190)^+$ pair does not immediately trigger proton release. This allows $Y_Z^\bullet$ to be metastably formed, giving rise to the $S_0Y_Z^\bullet$ and $S_1Y_Z^\bullet$ species, and the corresponding split signals.

As for the induction of split signals via the Mn-centered mechanism from both the S_2 and S_3 states across both the visible and NIR regions, the stability of $Y_Z^\bullet(His190)^+$ formation is again a crucial factor, together with the relative reduction potentials of $Y_Z^\bullet/Y_Z$ and the cluster in the S state in question (Figure 5). While the $CaMn_4$ cluster in the ground state is unable to oxidize Y_Z, the excited $CaMn_4$ cluster in the S_2 and S_3 states becomes sufficiently oxidizing to do so at cryogenic temperatures[21,25,54] (Figure 5A; a schematic of the relative redox potentials is shown in Figure 5B). Because an electron is now transferred to the $CaMn_4$ cluster at the same time as the $Y_Z^\bullet(His190)^+$ pair is formed, the charge on the cluster is lowered, and the unfavorable electrostatic interaction between these two species is avoided. Therefore, the $Y_Z^\bullet(His190)^+$ pair can be metastably formed, and a split signal can be induced. This is in direct contrast to a P_{680}-centered mechanism for the S_2 and S_3 states (Figure 4A), where the cluster maintains a charge of +1 relative to the S_1 state, thereby hindering formation of a stable $Y_Z^\bullet(His190)^+$ pair.

In the case of the S_0 and S_1 states (independent of the wavelength used for illumination), it would seem that even the excited cluster does not become sufficiently oxidizing to oxidize Y_Z (Figure 5B), thereby preventing the formation of $Y_Z^\bullet$ via this Mn-centered mechanism (Figure 5C). This is reasonable given that the resulting $CaMn_4$ cluster would be over-reduced compared to both the dark-stable S_1 and S_0 states.

Via examination of the environment of the $Y_Z^\bullet(His190)^+$ pair that would be formed by cryogenic illumination of PSII in the different S states according to the two different possible mechanisms, we have arrived at a unifying model that explains the pattern of induction behavior as summarized in Table 2.

dx.doi.org/10.1021/bi2015794 | *Biochemistry* 2012, 51, 2054−2064

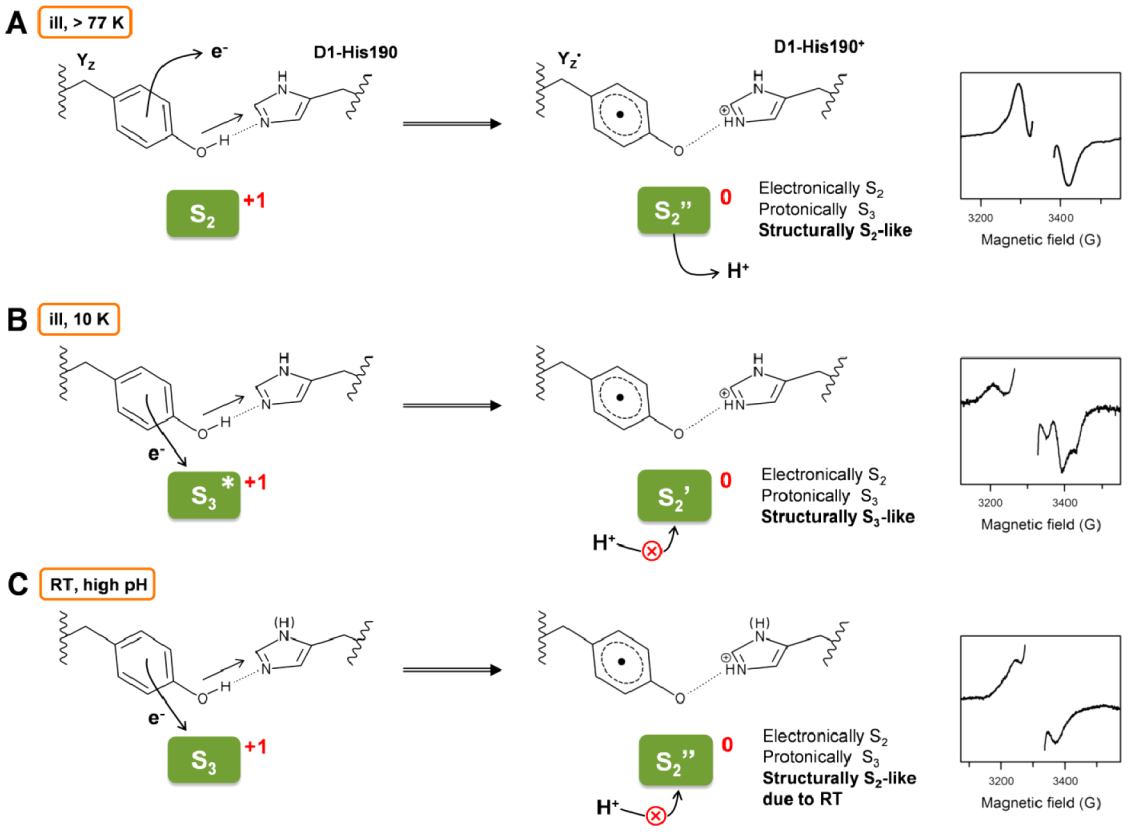

Figure 6. Mechanisms for the induction of S_2 state intermediates by (A) illumination with visible light at higher temperatures (>77 K), (B) illumination with NIR light at 10 K, or (C) incubation at high pH at room temperature in the dark. As in Figure 4, the electron and proton movements associated with the oxidation of Y_Z are shown in the reaction schemes. The transfers (allowed or blocked) of protons to and from the $CaMn_4$ cluster as a result of the formation of the $Y_Z^{\bullet}(His190)^+$ pair are also indicated. The characteristics of the resulting states upon split signal induction are summarized, and a representative EPR signal is shown for each state. The EPR spectrum in panel A was adapted with permission from ref 31. Copyright 2006 American Chemical Society. That in panel B was adapted with permission from ref 25. Copyright 2011 Elsevier. That in panel C was adapted with permission from ref 57. Copyright 2010 American Chemical Society.

The observation of the $(S_2)^{VIS}$ signal reported here and the determination of the Mn-centered mechanism for its induction have revealed a symmetry in the split signal induction pattern behavior, contrasting the S_0 and S_1 states against the S_2 and S_3 states. It is a symmetry that is reflected in the relative charges of the S states and has provided important support for the unified model focusing on electrostatics associated with the alternating electron and proton release pattern of the $CaMn_4$ cluster during the S state cycle. In the next two sections, the plausibility of this model and its utility in explaining other literature observations are demonstrated

Application of the Model. *(i) Split Signal after "Warm Trapping" Preillumination of the S_2 State.* The proposed model provides an alternative, and in our opinion more satisfactory, explanation for the reported induction of a 116 G wide split signal ($S_2Y_Z^{\bullet}$) from S_2 state centers that was induced via the P_{680}-centered mechanism after an initial preillumination under "warm" (77−190 K) conditions.[31,55] The authors proposed that the higher charge on the $CaMn_4$ cluster in the S_2 and S_3 states weakens the hydrogen bond between Y_Z and D1-His190, preventing the transfer of the phenolic proton of D1-His190 upon Y_Z oxidation at low temperatures. At higher temperatures, however, the energy barrier for this proton transfer is overcome, and the proton is trapped on D1-His190 or the neighboring D1-Asn298 upon the return to 10 K. The subsequent repeated induction of the split signal (even at 10 K) would then be possible because only an electron transfer is now involved, leading to the $Y_Z^{\bullet}/Y_Z^{-}$ redox couple, the proton lingering on His190 or Asn298.

We argue against such an explanation for two main reasons. First, in the case of split signal induction from the S_2 and S_3 states by NIR illumination, for which the Mn-centered mechanism is uncontroversial, the signals can be induced even without preillumination at higher temperatures. Even though Y_Z is now oxidized by the excited $CaMn_4$ cluster rather than excited P_{680}, the transfer of an electron from Y_Z would still entail a concomitant proton transfer across the suggested weakened H-bond to D1-His190 (Figure 5A). This occurs despite the higher charge of the S_2 and S_3 states before NIR illumination.[b]

Second, as mentioned, if the proton is trapped on either D1-His190 or D1-Asn298 after the preillumination, a $Y_Z^{\bullet}/Y_Z^{-}$ couple would be required for repeated reinduction of the signal at 10 K. However, this would lead to the negatively charged Y_Z^{-} being placed ∼3 Å from the positively charged $(D1\text{-}His190)^+$, or alternatively ∼7 Å from a charged $(D1\text{-}Asn298)^+$. It is difficult to envisage that such a closely placed charge pair would be stable enough to allow the repeated inductions of the split S_2 signal, even at 10 K. In addition, Y_Z^{-} is a very strong base, with a pK_a of approximately −2 (from ref 56) under normal conditions, and possibly even lower in the vicinity of the $CaMn_4$ cluster. It therefore seems unlikely that Y_Z^{-} would be sufficiently stable for the repeated inductions as seen in ref 31.

dx.doi.org/10.1021/bi2015794 | *Biochemistry* 2012, 51, 2054−2064

Instead, we propose the higher-temperature illumination [and $Y_Z^{\bullet}(His190)^+$ pair formation] allows the release of the proton from the $CaMn_4$ cluster in the S_2 state that is otherwise blocked (Figure 6A). This proton release then removes the unfavorable electrostatic interaction between the $Y_Z^{\bullet}(His190)^+$ pair and the cluster that prevented (meta)stable $Y_Z^{\bullet}$ formation. The transfer of an electron between the cluster and $Y_Z^{\bullet}$ is nevertheless blocked,[36] leading to the formation of $S_2''Y_Z^{\bullet}$ and the observed split signal [S_2'' indicates a proton-deficient S_2 state (see below for the difference between S_2' and S_2'')]. When the signal decays because of recombination of $Y_Z^{\bullet}$ with Q_A^-, the S_2 state is recovered. This interpretation remains consistent with the observed[31] recovery of the S_2 multiline signal intensity upon split signal decay (in contrast to the lack of recovery of multiline intensity observed after split signal formation via the Mn-centered mechanism, discussed above).

Note that we do not disagree with the proposal in ref 31 that a split signal originating from centers formally in the S_2 state ($S_2Y_Z^{\bullet}$) is induced by the warm preillumination protocol. Rather, we offer an alternative model to explain the induction behavior, without invoking the weakening of a hydrogen bond or a $Y_Z^{\bullet}/Y_Z^-$ couple.

(ii) Identification of Different Trapped Intermediates during the $S_2 \rightarrow S_3$ Transition. On the basis of the model presented here and as an extension to previous discussions about the split S_3 signal,[25,32,57] we propose that two distinct S state intermediates can in fact be trapped for the $S_2 \rightarrow S_3$ transition through the use of different signal induction protocols.

As discussed previously, split signal induction from the S_3 state by either visible or NIR illumination gives rise to an $S_2'Y_Z^{\bullet}$ species[19,21,54,58] via the Mn-centered mechanism.[25,32] S_2' signifies a cluster that is formally the same as the S_2 state electronically but is deficient by one proton (i.e., protonically S_3) from to the lack of proton recovery due to the low temperatures used (Figure 6B).

These $(S_3)^{VIS}$ and $(S_3)^{NIR}$ split signals have highly asymmetric line shapes (Figure 6B), in stark contrast to the symmetrical, 116 G wide spectrum (Figure 6A) that is induced by visible illumination of the S_2 state after a warm preillumination.[31] This is despite the fact that both split signal induction protocols should lead to a $CaMn_4$ cluster that is formally in the S_2 state electronically, but in the S_3 state protonically. This divergence in line shapes can be compared to the almost identical line shapes of the $(S_1)^{VIS}$, $(S_2)^{VIS}$, and $(S_2)^{NIR}$ split signals, all stemming from the $S_1Y_Z^{\bullet}$ species.

How can the very different line shapes of the $S_2 \rightarrow S_3$ intermediates be reconciled? The answer most likely lies in the resulting structure of the $CaMn_4$ cluster for each of these protocols. As the two protocols begin with the $CaMn_4$ cluster in different S states (S_2 for warm preillumination and S_3 for cryogenic NIR illumination), the respective starting structures of the clusters are significantly different.[46] At the low temperatures used, any significant structural rearrangement of the cluster is probably blocked. Therefore, although both protocols lead to a cluster that is electronically in the S_2 state and protonically in the S_3 state, the S_2 state warm preillumination protocol gives a cluster that is structurally S_2-like, whereas cryogenic illumination of the S_3 state gives a cluster that is structurally S_3-like (labeled S_2'' and S_2' in Figure 6, respectively). These structural differences would lead to different magnetic couplings that could explain the different split signal line shapes upon interaction with the $Y_Z^{\bullet}$ radical.

The analysis described above finds further correspondence in the split signal reported by Geijer et al.[59] induced from S_3 state samples at high pH (Figure 6C). It was proposed that the alkaline pH led to shifts in the relative redox potentials of the $Y_Z^{\bullet}/Y_Z$ and S_3/S_2 couples, allowing the S_3 state cluster to oxidize Y_Z in the dark at room temperature. The characteristics of this signal are very similar to those of the warm preillumination split signal ($S_2''Y_Z^{\bullet}$). Extending the discussion in ref 59 then, although the room-temperature conditions used there would technically allow the $CaMn_4$ cluster to regain a proton after oxidizing Y_Z, the lack of available protons due to the high pH prevents this (Figure 6C). This leads to a cluster that remains protonically S_3, though electronically S_2. Importantly here, structural rearrangement would now be allowed at room temperature, and given the close resemblance in both symmetry and width [~125 G (Figure 6A,C)] to the warm preillumination $S_2''Y_Z^{\bullet}$ signal, it would seem that the resulting structure is something that (at least magnetically) resembles the S_2 state of the $CaMn_4$ cluster (therefore also denoted $S_2''Y_Z^{\bullet}$ in Figure 6C).

CONCLUSIONS

We have reported the observation and characterization of an $(S_2)^{VIS}$ split signal that is directly induced from the S_2 state at 10 K using light in the visible wavelength region. As emphasized, our experimental results argue against this signal being attributable to residual S_1 state centers in the sample. Furthermore, the $S_1Y_Z^{\bullet}$ species formed via a Mn-centered mechanism is most likely responsible for this signal. The characteristics of the $(S_2)^{VIS}$ signal and its similarities to the $(S_2)^{NIR}$ split signal in terms of spectral shapes, $P_{1/2}$ values, and changes in S_2 multiline signal intensities before and after cryogenic illumination provide good support for this conclusion.

By considering the induction of the split signals in the different S states under different conditions, including $(S_2)^{VIS}$ (Table 2), we have arrived at a mechanistic model based on the stability of the $Y_Z^{\bullet}(His190)^+$ pair with respect to the charge of the $CaMn_4$ cluster. The split signal induction at different light qualities, temperatures, pH values, and S states could be explained using this simple yet wide-ranging model. Furthermore, it appears that two different $CaMn_4$ intermediates can be trapped for the $S_2 \rightarrow S_3$ transition depending on the split signal induction protocol used.

The mechanistic model proposed here is closely linked to the pattern of release of electrons and protons from the $CaMn_4$ cluster during the S cycle and further demonstrates the utility of the split signals in probing the immediate environment of the oxygen-evolving center in PSII.

AUTHOR INFORMATION

Corresponding Author

*Telephone: +46 18 471 6579. Fax: +46 18 471 6844. E-mail: felix.ho@kemi.uu.se.

Present Address

[†]Department of Physics, Freie Universität Berlin, Arnimallee 14, 14195 Berlin, Germany.

Funding

The Swedish Energy Agency, the Knut and Alice Wallenberg Foundation, The Carl Tryggers Foundation for Scientific Research, EU Program SOLAR-H2 (EU Contract 212508),

and Nordic Energy Research Program 06-Hydr-C13 are gratefully acknowledged for their financial support.

Notes

The authors declare no competing financial interest.

[a]Current data do not allow us to decide for sure whether the $Y_Z^{\bullet}(His190)^+$ pair is unable to form at all or is susceptible to rapid recombination. However, given that a time delay for proton release of ~200 μs after $Y_Z^{\bullet}$ formation has been reported for the $S_3 \rightarrow S_0$ transition,[53] recombination may be the more likely reason. Note that P_{680}-centered charge separation nevertheless takes place, despite it not being the mechanism behind the S_2 and S_3 split signals. Therefore, a likely recombination partner would be Q_A^-.

[b]Indeed, in ref 55, it was envisaged that the decay of the reported wider and shorter-lived component of this split signal involved the $Y_Z^{\bullet}(His190)^+ \rightarrow Y_Z(His190)^0$ reaction, entailing the transfer of a proton back across the hydrogen bond from His190 to $Y_Z^{\bullet}$ even at 10 K.

■ ABBREVIATIONS

DMSO, dimethyl sulfoxide; EPR, electron paramagnetic resonance; MES, (4-morpholino)ethanesulfonic acid; OEC, oxygen-evolving complex; $P_{1/2}$, microwave power at half-saturation; P_{680}, primary electron donor in PSII; NIR, near-infrared; $Pheo_{D1}$, pheophytin electron transport cofactor on the D1 subunit of PSII; PPBQ, phenyl-*p*-benzoquinone; PSII, Photosystem II; Q_A, quinone electron transport cofactor on the D2 subunit of PSII; Q_B, quinone electron transport cofactor on the D1 subunit of PSII; Y_D, Tyr160 in the D2 protein subunit of PSII; Y_Z, redox-active Tyr161 in the D1 protein of PSII; $Y_Z^{\bullet}$, radical of Y_Z.

■ REFERENCES

(1) Nelson, N., and Yocum, C. F. (2006) Structure and function of photosystems I and II. *Annu. Rev. Plant Biol. 57*, 521−565.

(2) Renger, G. (2008) Functional pattern of photosystem II. In *Primary processes of photosynthesis. Part 2* (Renger, G., Ed.) pp 237−290, Royal Society of Chemistry, Cambridge, U.K.

(3) Hays, A. M. A., Vassiliev, I. R., Golbeck, J. H., and Debus, R. J. (1998) Role of D1-His190 in proton-coupled electron transfer reactions in photosystem II: A chemical complementation study. *Biochemistry 37*, 11352−11365.

(4) Mamedov, F., Sayre, R. T., and Styring, S. (1998) Involvement of histidine 190 on the D1 protein in electron/proton transfer reactions on the donor side of photosystem II. *Biochemistry 37*, 14245−14256.

(5) Diner, B. A., and Britt, R. D. (2005) The redox-active tyrosines Y_Z and Y_D. In *The light-driven water:plastoquinone oxido-reductase in photosynthesis, advances in photosynthesis and respiration* (Wydrzynski, T., and Satoh, K., Eds.) pp 206−233, Springer, Dordrecht, The Netherlands.

(6) Styring, S., Sjöholm, J., and Mamedov, F. (2011) Two tyrosines that changed the world: Interfacing the oxidizing power of photochemistry to water splitting in photosystem II. *Biochim. Biophys. Acta 1817*, 76−87.

(7) McEvoy, J. P., and Brudvig, G. W. (2006) Water-splitting chemistry of photosystem II. *Chem. Rev. 106*, 4455−4483.

(8) Kok, B., Forbush, B., and McGloin, M. (1970) Cooperation of charges in photosynthetic O_2 evolution. I. A linear four step mechanism. *Photochem. Photobiol. 11*, 457−475.

(9) Dau, H., and Haumann, M. (2007) Time-resolved X-ray spectroscopy leads to an extension of the classical S-state cycle model of photosynthetic oxygen evolution. *Photosynth. Res. 92*, 327−343.

(10) Dau, H., and Haumann, M. (2007) Eight steps preceding O-O bond formation in oxygenic photosynthesis: A basic reaction cycle of the photosystem II manganese complex. *Biochim. Biophys. Acta 1767*, 472−483.

(11) Boussac, A., Zimmermann, J. L., and Rutherford, A. W. (1989) EPR signals from modified charge accumulation states of the oxygen-evolving enzyme in calcium-deficient photosystem II. *Biochemistry 28*, 8984−8989.

(12) Sivaraja, M., Tso, J., and Dismukes, G. C. (1989) A calcium-specific site influences the structure and activity of the manganese cluster responsible for photosynthetic water oxidation. *Biochemistry 28*, 9459−9464.

(13) MacLachlan, D. J., and Nugent, J. H. A. (1993) Investigation of the S_3 electron paramagnetic resonance signal from the oxygen-evolving complex of photosystem II: Effect of inhibition of oxygen evolution by acetate. *Biochemistry 32*, 9772−9780.

(14) Szalai, V. A., and Brudvig, G. W. (1996) Formation and decay of the S_3 EPR signal species in acetate-inhibited photosystem II. *Biochemistry 35*, 1946−1953.

(15) Baumgarten, M., Philo, J. S., and Dismukes, G. C. (1990) Mechanism of photoinhibition of photosynthetic water oxidation by chloride depletion and fluoride substitution: Oxidation of a protein residue. *Biochemistry 29*, 10814−10822.

(16) Andréasson, L.-E., and Lindberg, K. (1992) The inhibition of photosynthetic oxygen evolution by ammonia probed by EPR. *Biochim. Biophys. Acta 1100*, 177−183.

(17) Hallahan, B. J., Nugent, J. H. A., Warden, J. T., and Evans, M. C. W. (1992) Investigation of the origin of the "S3" EPR signal from the oxygen-evolving complex of photosystem 2: The role of tyrosine Z. *Biochemistry 31*, 4562−4573.

(18) Koulougliotis, D., Shen, J. R., Ioannidis, N., and Petrouleas, V. (2003) Near-IR irradiation of the S_2 state of the water oxidizing complex of photosystem II at liquid helium temperatures produces the metalloradical intermediate attributed to $S_1Y_Z^{\bullet}$. *Biochemistry 42*, 3045−3053.

(19) Nugent, J. H., Turconi, S., and Evans, M. C. (1997) EPR investigation of water oxidizing photosystem II: Detection of new EPR signals at cryogenic temperatures. *Biochemistry 36*, 7086−7096.

(20) Nugent, J. H., Muhiuddin, I. P., and Evans, M. C. (2002) Electron transfer from the water oxidizing complex at cryogenic temperatures: The S_1 to S_2 step. *Biochemistry 41*, 4117−4126.

(21) Ioannidis, N., and Petrouleas, V. (2000) Electron paramagnetic resonance signals from the S_3 state of the oxygen-evolving complex. A broadened radical signal induced by low-temperature near-infrared light illumination. *Biochemistry 39*, 5246−5254.

(22) Zhang, C., and Styring, S. (2003) Formation of split electron paramagnetic resonance signals in photosystem II suggests that $tyrosine_Z$ can be photooxidized at 5 K in the S_0 and S_1 states of the oxygen-evolving complex. *Biochemistry 42*, 8066−8076.

(23) Havelius, K. G. V., Su, J. H., Feyziyev, Y., Mamedov, F., and Styring, S. (2006) Spectral resolution of the split EPR signals induced by illumination at 5 K from the S_1, S_3, and S_0 states in photosystem II. *Biochemistry 45*, 9279−9290.

(24) Zhang, C., Boussac, A., and Rutherford, A. W. (2004) Low-temperature electron transfer in photosystem II: A tyrosyl radical and semiquinone charge pair. *Biochemistry 43*, 13787−13795.

(25) Havelius, K. G. V., Ho, F., Su, J.-H., Han, G., Mamedov, F., and Styring, S. (2011) The formation of the split EPR signal from the S_3 state of photosystem II does not involve primary charge separation. *Biochim. Biophys. Acta 1807*, 11−21.

(26) Havelius, K. G. V., Sjöholm, J., Ho, F., Mamedov, F., and Styring, S. (2010) Metalloradical EPR signals from the $Y_Z^{\bullet}$S-state intermediates in photosystem II. *Appl. Magn. Reson. 37*, 151−176.

(27) Hoganson, C. W., and Babcock, G. T. (1988) Electron-transfer events near the reaction center in O_2-evolving photosystem-II preparations. *Biochemistry 27*, 5848−5855.

(28) Rappaport, F., Blanchard-Desce, M., and Lavergne, J. (1994) Kinetics of electron transfer and electrochromic change during the redox transitions of the photosynthetic oxygen-evolving complex. *Biochim. Biophys. Acta 1184*, 178−192.

(29) Razeghifard, M. R., Klughammer, C., and Pace, R. J. (1997) Electron paramagnetic resonance kinetic studies of the S states in spinach thylakoids. *Biochemistry 36*, 86−92.
(30) Su, J. H., Havelius, K. G. V., Ho, F. M., Han, G., Mamedov, F., and Styring, S. (2007) Formation spectra of the EPR split signals from the S_0, S_1, and S_3 states in photosystem II induced by monochromatic light at 5 K. *Biochemistry 46*, 10703−10712.
(31) Ioannidis, N., Zahariou, G., and Petrouleas, V. (2006) Trapping of the S_2 to S_3 state intermediate of the oxygen-evolving complex of photosystem II. *Biochemistry 45*, 6252−6259.
(32) Boussac, A., Sugiura, M., Lai, T.-L., and Rutherford, A. W. (2008) Low-temperature photochemistry in photosystem II from *Thermosynechococcus elongatus* induced by visible and near-infrared light. *Philos. Trans. R. Soc. London, Ser. B 363*, 1203−1210.
(33) Berthold, D. A., Babcock, G. T., and Yocum, C. F. (1981) A highly resolved, oxygen-evolving photosystem II preparation from spinach thylakoid membranes. *FEBS Lett. 134*, 231−234.
(34) Völker, M., Ono, T., Inoue, Y., and Renger, G. (1985) Effect of trypsin on PS II particles: Correlation between Hill-activity, Mn-abundance and peptide pattern. *Biochim. Biophys. Acta 806*, 25−34.
(35) Arnon, D. I. (1949) Copper enzymes in isolated chloroplasts. Polyphenoloxidase in *Beta vulgaris*. *Plant Physiol. 24*, 1−15.
(36) Styring, S., and Rutherford, A. W. (1988) Deactivation kinetics and temperature-dependence of the S-state transitions in the oxygen-evolving system of photosystem II measured by EPR spectroscopy. *Biochim. Biophys. Acta 933*, 378−387.
(37) Han, G., Ho, F. M., Havelius, K. G. V., Morvaridi, S. F., Mamedov, F., and Styring, S. (2008) Direct quantification of the four individual S states in photosystem II using EPR spectroscopy. *Biochim. Biophys. Acta 1777*, 496−503.
(38) Beinert, H., and Orme-Johnson, W. H. (1967) in *Magnetic Resonance in Biological Systems* (Ehrenberg, A., Malmström, B. G., and Vänngård, T., Eds.) pp 221−247, Pergamon Press, Oxford, U.K.
(39) Sahlin, M., Gräslund, A., and Ehrenberg, A. (1986) Determination of relaxation times for a free radical from microwave saturation studies. *J. Magn. Reson. 67*, 135−137.
(40) Hirsh, D. J., Beck, W. F., Innes, J. B., and Brudvig, G. W. (1992) Using saturation-recovery EPR to measure distances in proteins: Applications to photosystem II. *Biochemistry 31*, 532−541.
(41) Brudvig, G. W., Casey, J. L., and Sauer, K. (1983) The effect of temperature on the formation and decay of the multiline EPR signal species associated with photosynthetic oxygen evolution. *Biochim. Biophys. Acta 723*, 366−371.
(42) Ho, F. M., Morvaridi, S. F., Mamedov, F., and Styring, S. (2007) Enhancement of $Y_D^{\bullet}$ spin relaxation by the $CaMn_4$ cluster in photosystem II detected at room temperature: A new probe for the S-cycle. *Biochim. Biophys. Acta 1767*, 5−14.
(43) Boussac, A., Girerd, J. J., and Rutherford, A. W. (1996) Conversion of the spin state of the manganese complex in photosystem II induced by near-infrared light. *Biochemistry 35*, 6984−6989.
(44) Boussac, A., Un, S., Horner, O., and Rutherford, A. W. (1998) High-spin states ($S \geq 5/2$) of the photosystem II manganese complex. *Biochemistry 37*, 4001−4007.
(45) Petrouleas, V., Koulougliotis, D., and Ioannidis, N. (2005) Trapping of metalloradical intermediates of the S-states at liquid helium temperatures. Overview of the phenomenology and mechanistic implications. *Biochemistry 44*, 6723−6728.
(46) Haumann, M., Muller, C., Liebisch, P., Iuzzolino, L., Dittmer, J., Grabolle, M., Neisius, T., Meyer-Klaucke, W., and Dau, H. (2005) Structural and oxidation state changes of the photosystem II manganese complex in four transitions of the water oxidation cycle ($S_0 \rightarrow S_1$, $S_1 \rightarrow S_2$, $S_2 \rightarrow S_3$, and $S_{3,4} \rightarrow S_0$) characterized by X-ray absorption spectroscopy at 20 K and room temperature. *Biochemistry 44*, 1894−1908.
(47) Klauss, A., Krivanek, R., Dau, H., and Haumann, M. (2009) Energetics and kinetics of photosynthetic water oxidation studied by photothermal beam deflection (PBD) experiments. *Photosynth. Res. 102*, 499−509.
(48) Lavergne, J., and Junge, W. (1993) Proton release during the redox cycle of the water oxidase. *Photosynth. Res. 38*, 279−296.
(49) Bernat, G., Morvaridi, F., Feyziyev, Y., and Styring, S. (2002) pH dependence of the four individual transitions in the catalytic S-cycle during photosynthetic oxygen evolution. *Biochemistry 41*, 5830−5843.
(50) Suzuki, H., Sugiura, M., and Noguchi, T. (2005) pH dependence of the flash-induced S-state transitions in the oxygen-evolving center of photosystem II from *Thermosynechoccocus elongatus* as revealed by Fourier transform infrared spectroscopy. *Biochemistry 44*, 1708−1718.
(51) Umena, Y., Kawakami, K., Shen, J.-R., and Kamiya, N. (2011) Crystal structure of oxygen-evolving photosystem II at a resolution of 1.9 Å. *Nature 473*, 55−60.
(52) Gerencsér, L., and Dau, H. (2010) Water oxidation by photosystem II: H_2O−D_2O exchange and the influence of pH support formation of an intermediate by removal of a proton before dioxygen creation. *Biochemistry 49*, 10098−10106.
(53) Haumann, M., Liebisch, P., Muller, C., Barra, M., Grabolle, M., and Dau, H. (2005) Photosynthetic O_2 formation tracked by time-resolved X-ray experiments. *Science 310*, 1019−1021.
(54) Ioannidis, N., Nugent, J. H., and Petrouleas, V. (2002) Intermediates of the S_3 state of the oxygen-evolving complex of photosystem II. *Biochemistry 41*, 9589−9600.
(55) Chrysina, M., Zahariou, G., Sanakis, Y., Ioannidis, N., and Petrouleas, V. (2011) Conformational changes of the $S_2Y_Z^{\bullet}$ intermediate of the S_2 to S_3 transition in photosystem II. *J. Photochem. Photobiol., B 104*, 72−79.
(56) Dixon, W. T., and Murphy, D. (1976) Determination of the acidity constants of some phenol radical cations by means of electron spin resonance. *J. Chem. Soc., Faraday Trans. 2* (72), 1221−1230.
(57) Sjöholm, J., Havelius, K. G. V., Mamedov, F., and Styring, S. (2010) Effects of pH on the S_3 state of the oxygen evolving complex in photosystem II probed by EPR split signal induction. *Biochemistry 49*, 9800−9808.
(58) Ioannidis, N., and Petrouleas, V. (2002) Decay products of the S_3 state of the oxygen-evolving complex of photosystem II at cryogenic temperatures. Pathways to the formation of the $S = 7/2$ S_2 state configuration. *Biochemistry 41*, 9580−9588.
(59) Geijer, P., Morvaridi, F., and Styring, S. (2001) The S_3 state of the oxygen-evolving complex in photosystem II is converted to the $S_2Y_Z^{\bullet}$ state at alkaline pH. *Biochemistry 40*, 10881−10891.